Anomalous Motion of a Sphere upon Impacting a Quiescent Liquid: Influence of Surface Wettability

Prasanna Kumar Billa, Tejaswi Josyula, and Pallab Sinha Mahapatra

1 Introduction

Understanding the dynamics of a solid impacting on liquids is of importance in broad areas of engineering, sports, and industries, such as drag reduction of swimmers and divers, entry and exit of the oars from the earth, ship slamming, the impact of boat hulls on water, extreme waves, weather on oil platforms, the locomotion of water-walking creatures, ink-jet printing, and spray adhesives. Dredging of solid particles and waste water discharge is two important applications of the solid–liquid interaction.

One of the first studies reporting the impact of solids on quiescent liquids is by Worthington [1], where single-spark photography is used to investigate the motion of solid spheres descending vertically into the water. Later, Kuwabara et al. [2] studied the motion of a solid sphere impacting the water for the Reynolds number between 1500 and 40,000. The positions of the steel, glass, and nylon spheres are calculated from the successive photographs taken simultaneously with two cameras. Valladares et al. [3] investigated the motion of a solid sphere travelling through a viscous fluid numerically. To analyse the behaviour of different density materials, such as steel, lead, sand, and concrete, the Verlet algorithm is employed. Further, the terminal velocities of the spheres are computed inside the water and other viscous fluids by using the particle positions. Rubinow and Killer [4] numerically studied a spinning sphere moving in a stationary fluid. The Basset–Boussinesq–Oseen (BBO) equation is used for obtaining transverse forces acting on a sphere in a liquid. First-order Stokes approximation is employed to obtain the position of the sphere. Particle

P. K. Billa · T. Josyula · P. S. Mahapatra (✉)
Micro Nano Bio Fluidics Group, Indian Institute of Technology Madras, Chennai 600036, India
e-mail: pallab@iitm.ac.in

T. Josyula
Institute for Technical Thermodynamics, Technical University of Darmstadt, 64287 Darmstadt, Germany

image velocimetry (PIV) experiments and Lattice–Boltzmann (LB) simulations on a single sphere settling under gravity are investigated by Ten Cate et al. [5]. A sediment sphere (Nylon) is used to study the behaviour under silicon oil of different viscosities. They have studied the sphere trajectories, flow field, and velocity for low Reynolds numbers ($Re = 1.5$–31.9) and low Stokes numbers (0.2–4). Total forces acting on a sphere and torque are investigated using LB simulations, and the sphere trajectories are observed experimentally with PIV. A complete study of the negatively and positively buoyant rigid spheres are reported by Horowitz et al. [6]. Different release techniques are used depending on the density ratio. The sphere with a density greater than the impacting liquid uses a top-releasing mechanism. A bottom-releasing mechanism is used for spheres with densities lower than the target liquid. An extensive study is conducted on vortex formation in the wake and the behaviour of spheres inside the liquid. According to the motion of the sphere, regime maps are used to visualise the wakes and trajectories of freely falling and rising spheres. For various Re, vorticity measurements and drag coefficients are studied. The major regimes of the sphere motions are as follows: vertical, oblique, intermittent oblique, and zigzag. Wake-induced oscillatory paths of the sphere, cylinder, and disk are investigated by Ern et al. [7]. The transverse displacement oscillations are observed for the various Reynolds numbers. Will and Krug [8] studied the dynamics of freely rising spheres and the effect of the moment of inertia in quiescent and turbulent fluids. A complete analytical solution of the sphere falling through the liquid is given by Guo [9] for various Reynolds numbers for the nonzero initial velocity. They have considered a rectilinear fall of a sphere onto a quiescent fluid. The BBO equation is solved for the acceleration of the spheres inside the viscous liquid. Hydrodynamic interactions of solid particles are studied by Mahapatra et al. [10], Harikrishnan et al. [11], Theofanous et al. [12]. Dredging of solid particles and waste water discharge is investigated by Carr et al. [13]. Using various analytical techniques, Nouri et al. [14] carried out a comprehensive study on the sedimentation of spherical particles in Newtonian fluid media. They presented three simple and exact analytical models for the problem of resolving the nonlinear equation of sedimentation. Lead, copper, and aluminium are impacted onto the water and solve the unsteady motion of the particle with the BBO equation by neglecting the Basset force. It is concluded that the analytical methods and numerical methods are able to predict the positions, velocities, and accelerations of the particles falling through the water. The impact of a solid mass on a transient cavity of air has been explored by Duclaux et al. [15]. For steel spheres, the formation of a transitory cavity for materials with carbon soot on their surfaces is explored. The effect of the cavity on the radius, density, and radius of the releasing sphere and cylinder is thoroughly discussed. Also, they constructed an analytical model to investigate the theoretical radius of the cavity as a function of time and the density of the releasing solid. The authors used potential flow to calculate cavity formation inside the liquid at various intervals. After impacting the quiescent liquid, the solid sphere entrains an air cavity behind the sphere. The formation of pinch-offs and cavity ripples is investigated by Louf et al. [16]. However, the authors have not discussed the dynamics of the sphere and how the surface wettability affects the

sphere trajectories. It is essential to study the effect of surface wettability modification on the dynamics of the sphere.

The main goal of this study is to systematically investigate the effect of impact conditions and effective parameters on the underwater behaviour of a solid sphere. The experimental outcomes reveal that, while a sphere with higher density ($\rho/\rho_l \geq 7.926$) descends in a straight path, a sphere with lower density ($\rho/\rho_l \leq 2.771$) deviates from its vertical impact position. Additionally, a polynomial equation is used to investigate distinct stages in the evolution of penetration depth as a sphere moves through the quiescent water. The transition length l_t, at which the transition occurs, i.e., the trajectory of the sphere deviates from a straight line path, is delineated for all the cases. It is evident that this l_t is greatly influenced by the diameter of the sphere. Lastly, we demonstrate here that the observed anomalous motion of low-density spheres can be controlled by modifying the surface wettability of the sphere. It is observed that a superhydrophobic sphere of lower density follows a straight line path, which is attributed to the formation of an air cavity in the wake. Further, a superhydrophobic sphere moves faster than a non-coated sphere in quiescent water.

2 Experimental Setup and Methodology

A. Experimental setup

A schematic of the experimental setup is shown in Fig. 1a. The spheres are released into a water tank of $200 \times 200 \times 400$ mm, which is made of clear, translucent acrylic material. A vacuum system is used to release the sphere with varying density and diameter, as shown in Fig. 1. This vacuum system is designed to create an impacting condition with zero initial velocity while ensuring no rotation is imparted onto the sphere. This is confirmed by observing the trajectory of the sphere prior to the impact on the liquid–air interface. Figure 1b shows various time instants during the motion of a sphere, with a black mark on the surface after the release from the pipette tip. A constant location of the black mark at different time instants highlights that there is no rotation of the sphere in the air before the impact. Before conducting the experiment, the water tank and the spheres are cleaned using isopropyl alcohol and ethanol. The length and width of the water tank are 20 times that of the diameter of the largest sphere used in the experiment. This results in a negligible influence of the walls of the tank on the trajectory of the spheres. All the experiments are conducted in a closed room with an ambient temperature of 25 ℃. An optical table (HOLMARC, India) is used to support the experimental apparatus, providing mobility and a vibration-free base.

The motion of the sphere inside the liquid is recorded using a Phantom High-Speed camera (VEO E-340L) with a Nikon Micro 60 mm lens. The camera records images at a rate of 1000 frames per second with a resolution of 768×1024 pixels and an exposure period of 990 μs. A 15-W recessed panel light is used to illuminate the back side of the tank.
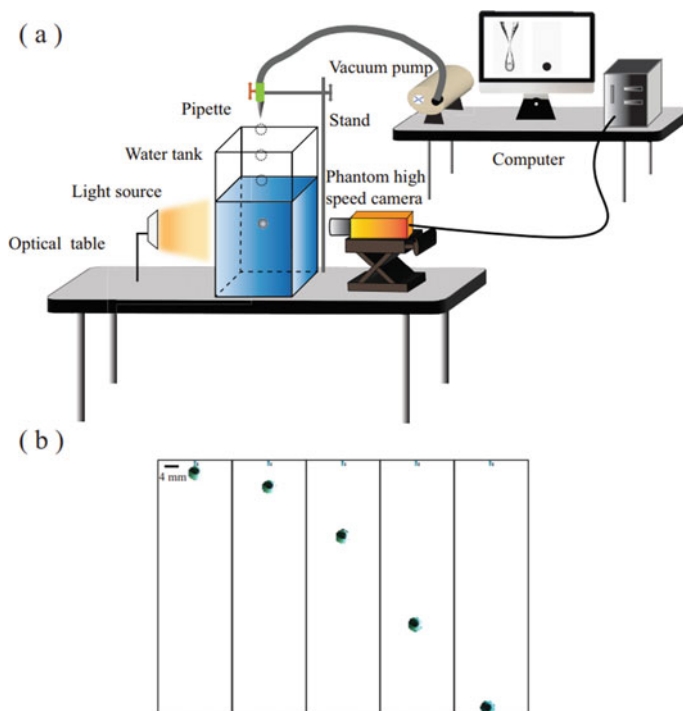
(a)

(b)

Fig. 1 (**a**) Schematic of the experimental setup and (**b**) Chronophotography of a sphere travelling in the air following the release from a pipette tip. The time step between the consecutive images is 33.33 ms

B. **Methodology**

Preparation of SH spheres:

A commercially available coating spray (NeverWet spray) is used to render the surface of the spheres as superhydrophobic. NeverWet spray is a two-step product system designed to create moisture repelling barrier on a variety of substrates. The following is the procedure for modifying the surface wettability of the sphere. The spheres are placed in a clean petri dish and are arranged so that they do not come into contact with each other or the wall. First, the base coat is applied, followed by the application of the top coat. The base coating is sprayed twice, and the spheres are then placed in the petri dish for one minute. A toothpick is then used to disperse the spheres. The process is repeated on the opposite surface of the spheres. The spheres are cured at ambient temperature for 30 min before applying the top coating in the same procedure followed for the base coat. The spheres are then placed in a dry environment for 12 h before doing the experiment. This results in a high water repellent surface.

In the present study, polytetrafluroethylene (PTFE), glass, and steel spheres are used, which are procured from local vendors. The mass of a sphere (M) is measured

Table 1 Properties of the spheres used in the present study

S. No.	Material	ρ/ρ_l	d (mm)
1	PTFE	2.167	4, 6, 10
2	Glass	2.771	4, 6, 10
3	Steel	7.926	4, 6, 10

using an electronic weighing machine, and by measuring the diameter using a Vernier Calliper, the volume of the sphere (V) is calculated. The density of the spheres (ρ) is then calculated as $\rho = \frac{M}{V}$. The measured densities are 2167, 2771, and 7926 kg/m^3, PTFE, glass, and steel, respectively. Three different diameters are considered for each material, as given in Table 1. In the present study, three different impact situations are considered by varying the distance above the air–water interface from which the spheres are released. Consequently, the impact Weber numbers ($We = \frac{\rho v^2 d}{2\sigma}$) range from 68.11 to 204.37. Here, v is the impact velocity of the sphere, d is the diameter of the sphere, μ is the dynamic viscosity (0.89 mPa) of the water at 25°C, ρ_l is the density of water (1000 kg/m^3), g is gravitational acceleration (9.81 m/s^2), and σ is surface tension of the air–water interface (0.072 N/m).

The captured images from the high-speed camera are post-processed using ImageJ and MATLAB. Briefly, the background is subtracted from each image, and then, by thresholding based on the intensity, the location of the sphere is identified. Followed by this, the penetration depth (PD) is extracted by tracking the centre of the sphere.

3 Results and Discussion

Figure 2 shows the motion of non-coated rigid spheres of different densities after impacting quiescent water, using the snapshots captured by the high-speed camera at different time instants. The effect of density is highlighted here by presenting the trajectories of spheres varying density, for a fixed sphere diameter and *We*. First, Fig. 2a depicts the chronophotography of a sphere with $\rho/\rho_l = 7.926$. It is observed that the sphere moves in a straight line (black dashed line) without deviating from its initial impact point. Such a behaviour is expected for a sphere whose density is much larger than the liquid, and is in line with previous reports. This straight line trajectory of the sphere is further depicted in the figure in the last snapshot. Figure 2b depicts the chronophotography of spheres with $\rho/\rho_l = 2.771$. It is observed that the sphere ($\rho/\rho_l = 2.771$) is straying away from a straight line path. The same phenomenon is observed for spheres with $\rho/\rho_l = 2.167$, as shown in Fig. 2c. Due to the high impact Weber number (*We* > 68), the wake of the sphere forms a wave motion in a plane containing its streamwise axis (Taneda [17]). This wake rotates slowly about that axis, resulting in a change in the path of the sphere from straight to random. The formation of vortices and wave motion for the different Reynolds numbers is investigated by Horowitz et al. [6]. In the present investigation, for current
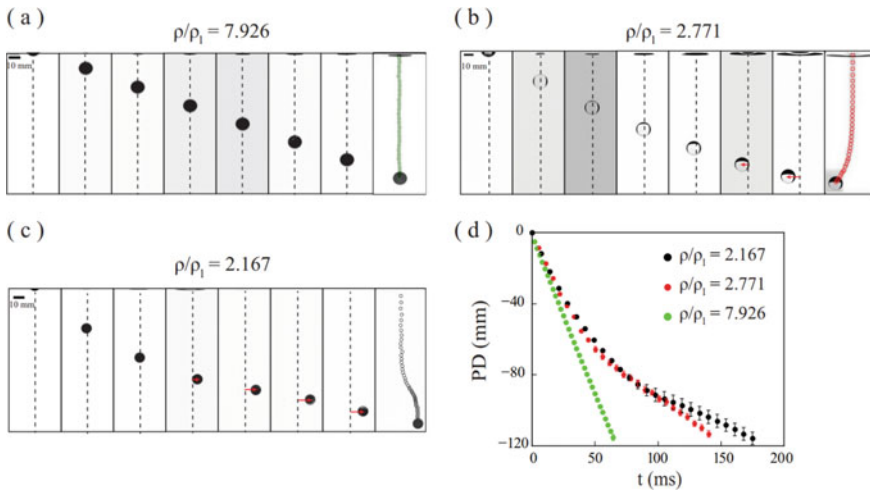
Fig. 2 Chronophotography of the impact of non-coated spheres with 10 mm diameter is shown for (**a**) Steel ($\rho/\rho_l = 7.926$) (**b**) Glass ($\rho/\rho_l = 2.771$) and, **c** PTFE ($\rho/\rho_l = 2.167$), at an impact We of 204.37. The time duration between consecutive images is 8 ms for (**a**), 15 ms for (**b**), and 30 ms for (**c**). For the respective cases presented in (**a**), (**b**) and (**c**), (**d**) show the (PD) of the sphere with time (t). The black dashed line illustrates a straight path from the air–water interface during impact. The red arrow shows the deviation of the sphere from the vertical impact position, and the scatter points show the position of the centre of the sphere

We, lower density spheres deviate from a vertical impact position. The production of an asymmetric wake causes the sphere to deviate from the straight path.

The variation of the penetration depth with time for the cases presented in Fig. 2a–c is presented in Fig. 2d. By observing the trajectories and analysing the penetration depth of spheres with varying densities, this deviation in the trajectory is inversely correlated to the density of the sphere. The influence of vortices on a sphere with $\rho/\rho_l = 7.926$ is less than others due to the relatively higher density than the impacting liquid, which reduces the effect of the vortices in the wake of the sphere so that the penetration depth from the air–water interface increases linearly. For the non-coated spheres $\rho/\rho_l = 2.167$ and 2.771, the transition inside the fluid occurs at a precise point, where the sphere starts moving away from the vertical impact position. The wake of a sphere moves like a progressive wave in a plane where the streamwise axis passes through the middle of the sphere and moves abnormally in a different direction, as demonstrated in Fig. 2. The vortex loops diffuse rapidly at the wake of the sphere in the radial direction (randomly) as the impact velocity increases. As a result, a sphere impacting with high *We* on a quiescent liquid experiences a side force (oblique). The direction of this oblique force is entirely unpredictable. The sphere moves anomalously in a different direction, as demonstrated in Fig. 2a–c. The penetration depth increases nonlinearly from the air–water interface due to progressive wave motion in the wake of the spheres. It is also found that the time

required to reach a specific position is lower for the case of $\rho/\rho_l = 7.926$ than the lower density spheres (Fig. 2d).

Here, the deviation observed for lower density spheres is quantified in terms of the transition length (l_t). This l_t is the location at which the deviation in the path is observed. Taking a clue from Fig. 2d, where the maximum deviation is observed for the lowest density spheres considered, the effect of sphere diameter and *We* is presented for the case of spheres with the lowest density ($\rho/\rho_l = 2.167$). Overall, the diameter of the sphere has a greater influence on l_t, compared to *We* as shown in Fig. 3. For a fixed *We*, the transition length increases as the diameter of the sphere increases. The increase in mass of the sphere as diameter increases will help sustain the upward lift force generated due to the difference in densities between the sphere and the liquid. Hence, larger diameter spheres can further continue on a straight path compared to spheres with smaller diameters. Interestingly, the effect of *We* is negligible on the l_t. This can be explained by the fact that in the present study, *We* is varied by varying the height from which the sphere is released. Therefore, considering a smaller range of change in height employed in the present study, we believe the change in *We* is not significant to greatly influence the impact dynamics.

As mentioned before, one novel aspect of the present study is the detailed analysis of the anomalous motion resulting from a deviation in the path for spheres of low density. To further highlight this outcome, here, the evolution of the penetration depth is thoroughly analysed to understand the patterns in the overall evolution of the trajectories of impacting spheres. Overall, three distinct stages in the evolution of the penetration depth are observed, as shown in Fig. 4. These various stages are identified based on the velocity of the sphere during the descent. For $We = 68.11$, after impacting the liquid, the sphere accelerates quickly (stage 1). A quadratic polynomial ($PD = -1.0874 - 0.9526t + 0.0019t^2$) with a coefficient of determination of $R^2 = 0.99$ is used to fit stage 1 (blue colour) starting from 0 to 122 ms.

Fig. 3 For spheres with $\rho/\rho_l = 2.167$, the transition length l_t is plotted for different impact *We*. The effect of the diameter of the sphere is also presented. Evidently, the diameter of the sphere has a greater influence on the transition length when compared to the impact *We*
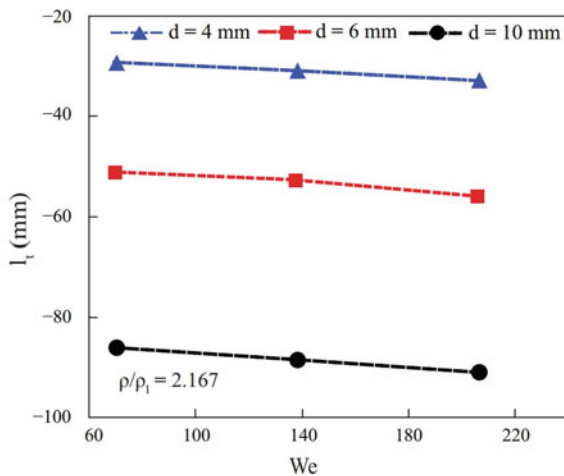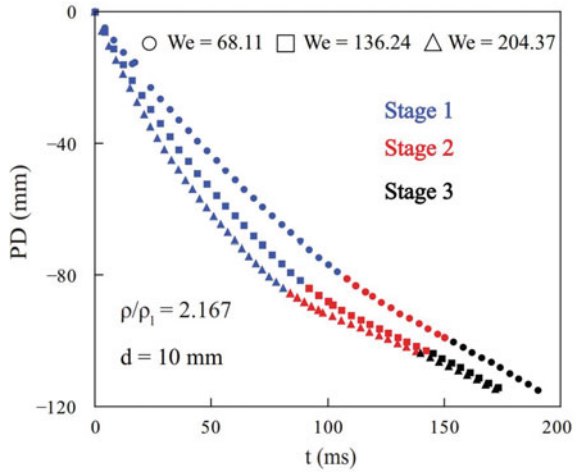
Fig. 4 Evolution of the penetration depth of a 10 mm diameter sphere with $\rho/\rho_l = 2.167$ is plotted for different impact *We*. Three distinct stages observed are plotted in different colours

When the sphere deviates from the straight path, the velocity of the sphere decreases gradually, as shown in Fig. 4. Stage 2 (red colour), starts at 122 ms and ends at 153 ms, where a quadratic polynomial ($PD = -1.6568 - 1.2438t + 0.0038t^2$) correctly explains the evolution of penetration depth. After deviating from the path, in stage 3 (black colour), the sphere moves with a constant velocity. This results in a linear increase in the penetration depth. This linear variation ($PD = -1.9379 - 1.4932t + 0.0015t^2$) of penetration depth in Stage 3 is further confirmed by conducting experiments with a larger field of view. Figure 4 also shows the effect of impact *We*. For brevity, the equations that fit the data are omitted for the higher We numbers. Overall, qualitatively, the three stages are observed here also. However, the total amount of time encompassing each of the stages reduces as the impact *We* increase. This is expected due to the fact that the kinetic energy of the sphere increases with increasing We, which results in a faster movement of the sphere inside the liquid. Similar stages are observed for other lower density ($\rho/\rho_l = 2.771$) spheres also. Lastly, for the cases of steel spheres, where no deviation in path is observed, the penetration depth increases in an almost linear fashion, as can also be seen in Fig. 2

Surface wettability modification is an emerging field of study with various advantages such as drag reduction and low contamination. Such wettability modification is previously studied for impinging spheres (McHale et al. [18], Jetly et al. [19], and Vakarelski et al. [20]). The entry of a surface wettability modified sphere in an air–water mixture is explored using Particle Image Velocimetry by Yuan et al. [21]. Here, we study the impacting scenario of spheres with superhydrophobic coating on their surface. Figure 5 illustrates the differences in how non-coated and SH-coated spheres behave when submerged in water. The trajectory of the path followed by the spheres is also plotted. As explained before, the non-coated sphere shows a deviation from the interface (see Fig. 5a). However, a superhydrophobic sphere follows a straight line path (see Fig. 5b). The black dashed line shows the straight path of the sphere ($\rho/\rho_l = 2.771$). The entrapped air causes an axisymmetric cavity in the wake of the
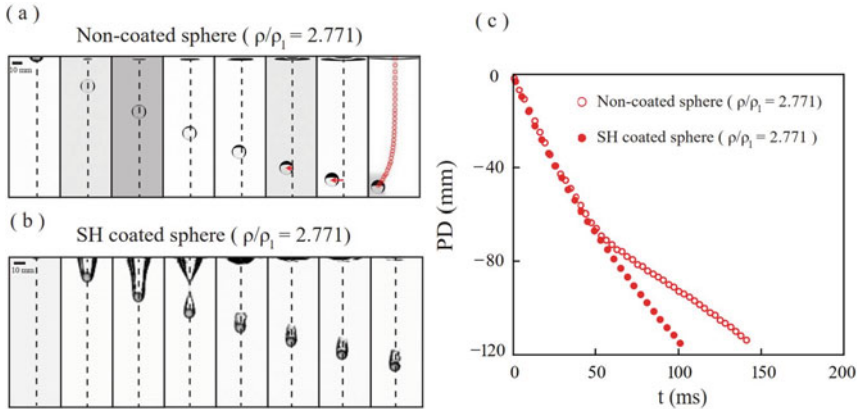
Fig. 5 Chronophotography of the impact of (**a**) non-coated and (**b**) superhydrophobic coated sphere ($\rho/\rho_l = 2.771$) with $d = 10$ mm and $We = 204.37$. The time step between two consecutive images in (**a**) and (**b**) is 15 ms. A comparison of the evolution of penetration depth for both cases is shown in (**c**)

sphere, due to which the SH-coated spheres (regardless of sphere density) follow a straight line path. Entrapped air in the wake of the sphere as it falls through the water prevents the creation of a vortex because of the Cassie-Baxter state, as explored by Aristoff et al. [22]. Also, the volume of the cavity (entrained) at the wake tries to keep the sphere from moving away from the vertical impact position. Further, for the same initial conditions, a superhydrophobic sphere moves with a higher velocity than a non-coated sphere, which is the result of the reduction in drag. The evolution of penetration depth of the non-coated sphere ($\rho/\rho_l = 2.771$) is depicted in Fig. 5c shows that the transition length of the SH-coated sphere is changed. The deviation of the sphere from the vertical impact position is not seen in SH-coated spheres because vortices will not directly act on the sphere. In SH-coated spheres, the three-stage behaviour of non-coated spheres changes is not observed in SH-coated sphere for the densities ($\rho/\rho_l \geq 1$).

4 Conclusions

A systematic experimental study is reported here showing the settling behaviour of rigid spheres of various densities. It is found that a deviation in path occurs for spheres with lower density ($\rho/\rho_l \leq 2.771$), where such a deviation is not observed for spheres with high density ($\rho/\rho_l \leq 7.926$). The transition length of a sphere, where the path of the sphere shows a deviation, depends more on the diameter and density than on the impact Weber number. Three distinct stages are observed in the evolution of the penetration depth, which is the distance from the air–water interface. As a future avenue of research, the radial random motion of the sphere can be examined

and quantified with precision by employing two high-speed cameras, each oriented orthogonally to the water tank.

One novel outcome from the present study is the difference in behaviour of descending spheres when the surface is superhydrophobic. The presence of an air-entrapped cavity in the wake of a superhydrophobic sphere results in axisymmetry of the flow field, resulting in a straight line path for the trajectory of the sphere. Further, the superhydrophobic spheres move faster than a non-coated sphere, which further affirms the previously reported ability of superhydrophobic surfaces decreasing the drag. Additionally, unlike a non-coated sphere, the trajectory of the superhydrophobic does not exhibit a three-stage behaviour.

Nomenclature

PD Penetration depth[mm]
d Diameter[mm]
l_t Transition length[mm]
t Time[ms]
ρ/ρ_1 Density ratio-
Re Reynolds number-
We Weber number

References

1. Arthur MW (1883) On impact with a liquid surface. Proc Roy Soc London 34:217–230
2. Kuwabara G, Chiba S, Kono K (1983) Anomalous motion of a sphere falling through water. J Phys Soc Jpn 52(10):3373–3381
3. Valladares RM, Goldstein P, Stern C, Calles A (2003) Simulation of the motion of a sphere through a viscous fluid. Rev Mex Fis 49(2):166–174
4. Rubinow SI, Joseph BK (1961) The transverse force on a spinning sphere moving in a viscous fluid. J Fluid Mech 11(3):447–459
5. Ten Cate A, Nieuwstad CH, Derksen JJ, Van den Akker HEA (2002) Particle imaging velocimetry experiments and latticeBotlzmann simulations on a single sphere settling under gravity. Phys Fluids 14(11):4012–4025
6. Horowitz M, Williamson CHK (2010) The effect of Reynolds number on the dynamics and wakes of freely rising and falling spheres. J Fluid Mech 651:251–294
7. Ern P, Risso F, Fabre D, Magnaudet J (2011) Wake-induced oscillatory paths of bodies freely rising or falling in fluids. Annu Rev Fluid Mech 44:97–121
8. Jelle W, Dominik K (2020) Rising and sinking in resonance: probing the critical role of rotational dynamics for buoyancy driven spheres. arXiv preprint arXiv:03643.

9. Guo J (2011) Motion of spheres falling through fluids. J Hydraul Res 49(1):32–41
10. Mahapatra PS, Manna NK, Ghosh K (2013) Hydrodynamic and thermal interactions of a cluster of solid particles in a pool of liquid of different Prandtl numbers using two-fluid model. Heat Mass Transf 49:1659–1679
11. Harikrishnan S, Pallab SM (2021) Effect of liquid–air interface on particle cloud dynamics in viscous liquids. Phys Fluids 33(6):063306
12. Theofanous TG, Yuen WW, Angelini S (1999) The verification basis of the PM-ALPHA code. Nucl Eng Design 189(1–3):59–102
13. Carr SA, Liu J, Tesoro AG (2016) Transport and fate of microplastic particles in wastewater treatment plants. Water Res 91:174–182
14. Nouri R, Ganji DD, Hatami M (2014) Unsteady sedimentation analysis of spherical particles in Newtonian fluid media using analytical methods. Propul Power Res 3(2):96–105
15. Duclaux V, Caille F, Duez C, Ybert C, Bocquet L, Clanet C (2007) Dynamics of transient cavities. J Fluid Mech 591:1–19
16. Louf J-F, Chang B, Eshraghi J, Mituniewicz A, Vlachos PP, Jung S (2018) Cavity ripple dynamics after pinch-off. J Fluid Mech 850:611–623
17. Taneda S (1978) Visual observations of the flow past a sphere at Reynolds numbers between 104 and 106. J Fluid Mech 85(1):187–192
18. McHale G, Shirtcliffe NJ, Evans CR, Newton MI (2009) Terminal velocity and drag reduction measurements on superhydrophobic spheres. Appl Phys Lett 94(6):1–4
19. Aditya J, Ivan UV, Sigurdur TT (2018) Drag crisis moderation by thin air layers sustained on superhydrophobic spheres falling in water. Soft Matter 14(9):1608–1613
20. Ivan UV, Evert K, Aditya J, Mohammad MM, Andres AA, Derek YC, Sigurdur TT (2017) Self determined shapes and velocities of giant near-zero drag gas cavities. Sci Adv 3(9):1–8
21. Yuan Q, Hong Y, Zhao Z, Gong Z (2022) Water–air two-phase flow during entry of a sphere into water using particle image velocimetry and smoothed particle hydrodynamics. Phys Fluids 34(3):032105
22. Jeffrey MA, John WMB (2009) Water entry of small hydrophobic spheres. J Fluid Mech 619:45–78